




MRI Clustering Reveals Three ALS Subtypes With Unique Neurodegeneration Patterns

Harold H. G. Tan, MD ¹, Henk-Jan Westeneng, MD,¹ Abram D. Nitert, MD,¹
 Kevin van Veenhuijzen, MD ¹, Jil M. Meier, PhD ¹, Hannelore K. van der Burgh, PhD,¹
 Martine J. E. van Zandvoort, PhD,^{1,2} Michael A. van Es, MD, PhD,¹
 Jan H. Veldink, MD, PhD,¹ and Leonard H. van den Berg, MD, PhD¹

Objective: The purpose of this study was to identify subtypes of amyotrophic lateral sclerosis (ALS) by comparing patterns of neurodegeneration using brain magnetic resonance imaging (MRI) and explore their phenotypes.

Methods: We performed T1-weighted and diffusion tensor imaging in 488 clinically well-characterized patients with ALS and 338 control subjects. Measurements of whole-brain cortical thickness and white matter connectome fractional anisotropy were adjusted for disease-unrelated variation. A probabilistic network-based clustering algorithm was used to divide patients into subgroups of similar neurodegeneration patterns. Clinical characteristics and cognitive profiles were assessed for each subgroup. In total, 512 follow-up scans were used to validate clustering results longitudinally.

Results: The clustering algorithm divided patients with ALS into 3 subgroups of 187, 163, and 138 patients. All subgroups displayed involvement of the precentral gyrus and are characterized, respectively, by (1) pure motor involvement (pure motor cluster [PM]), (2) orbitofrontal and temporal involvement (frontotemporal cluster [FT]), and (3) involvement of the posterior cingulate cortex, parietal white matter, temporal operculum, and cerebellum (cingulate-parietal-temporal cluster [CPT]). These subgroups had significantly distinct clinical profiles regarding male-to-female ratio, age at symptom onset, and frequency of bulbar symptom onset. FT and CPT revealed higher rates of cognitive impairment on the Edinburgh cognitive and behavioral ALS screen (ECAS). Longitudinally, clustering remained stable: at 90.4% of their follow-up visits, patients clustered in the same subgroup as their baseline visit.

Interpretation: ALS can manifest itself in 3 main patterns of cerebral neurodegeneration, each associated with distinct clinical characteristics and cognitive profiles. Besides the pure motor and frontotemporal dementia (FTD)-like variants of ALS, a new neuroimaging phenotype has emerged, characterized by posterior cingulate, parietal, temporal, and cerebellar involvement.

ANN NEUROL 2022;92:1030–1045

Amyotrophic lateral sclerosis (ALS) is a progressive neurodegenerative disease in which patients are confronted with speech impairment, muscle wasting and weakness, and eventually respiratory insufficiency and death.¹ With the increase in knowledge over the years, the

remarkable heterogeneity of ALS is becoming more apparent in many aspects of the disease, such as site of onset and rate of progression, the presence of cognitive and behavioral impairment, genetic predisposition, and pathological processes.¹ Life expectancy is also highly

View this article online at [wileyonlinelibrary.com](https://onlinelibrary.wiley.com/doi/10.1002/ana.26488). DOI: 10.1002/ana.26488

Received Mar 21, 2022, and in revised form Aug 18, 2022. Accepted for publication Aug 18, 2022.

Address correspondence to Dr Berg, Department of Neurology, G03.228, University Medical Center Utrecht, P.O. Box 85500, 3508 GA Utrecht, The Netherlands. E-mail: l.h.vandenberg@umcutrecht.nl

From the ¹Department of Neurology, UMC Utrecht Brain Center University Medical Center Utrecht, Utrecht University, Utrecht, The Netherlands; and ²Department of Experimental Psychology, Utrecht University, Utrecht, The Netherlands

Additional supporting information can be found in the online version of this article.

variable, ranging from a few months to more than 10 years.² This heterogeneity means that providing an accurate prognosis is complicated for clinicians and, as a result, leaves patients with uncertainty about their future. To advance our understanding of ALS, it is crucial to get to the core of this heterogeneity, in particular, because it seems highly likely that treatments will need to be tailored to individual patient characteristics.³ Yet, despite the strong appeal to move toward personalized medicine, it has proved difficult to grasp what underlies these differences in disease presentation; a unified framework to address this heterogeneity remains elusive.

Researchers have often opted for a one-dimensional approach in the form of subgroup stratification. Clinical stratification became apparent when poorer prognoses were first found in patients with a bulbar onset of symptoms.⁴ More clinical variables associated with survival have since been discovered, leading to the development of the European Network to Cure ALS (ENCALS) prediction model.² The discovery of the *C9orf72* hexanucleotide repeat expansion and its association with frontotemporal dementia (FTD), has similarly led to genetic patient stratification, showing associations with survival, cognitive and behavioral impairment, and extra-motor brain degeneration.⁵⁻⁷ Yet, it is unlikely that univariable approaches can fully capture underlying disease processes.¹ As an alternative, neuroimaging may provide an in vivo biomarker that consistently correlates to both clinical characteristics and genotypes.⁸ Hence, magnetic resonance imaging (MRI) might become an effective instrument to disentangle disease heterogeneity and provide biomarkers that identify subgroups.^{9,10}

Therefore, we stratified the ALS spectrum using multimodal neuroimaging data and propose subgroups of patients that share similar patterns of cerebral neurodegeneration detected by a probabilistic, unsupervised, network-based, clustering algorithm. We hypothesize that, without using prior information, the algorithm can find subgroups of patients which share similar patterns of brain involvement and display distinct disease characteristics.

Subjects/Materials and Methods

We included 488 patients with ALS and 338 controls between 2009 and 2020. Patients and controls were recruited from a population-based cohort, provided they did not have any contra-indications for an MRI scan (eg, severe swallowing difficulties and respiratory insufficiency when lying supine). Participants with structural brain abnormalities (eg, stroke or brain tumor) were excluded. In addition to baseline scans, a total of 512 follow-up scans were conducted in 275 patients at a 3 to 6-month

interval and a maximum of 4 scans per patient. Cross-sectional scans of controls were used as reference. In total, 1,338 MRI scans were used in the analyses. Demographic and clinical data were collected from the date of diagnosis. Patients were tested for *C9orf72* repeat expansion carriership.⁶ *UNC13A* single nucleotide polymorphism (SNP) data (rs12608932) from a previous study were used for a complete case analysis.⁷ The revised ALS functional rating scale (ALSFRS-R) was administered at each visit,¹¹ as well as the Dutch version of the Edinburgh cognitive and behavioral ALS screen (ECAS) starting from 2015.^{12,13} T1 and diffusion tensor imaging (DTI) MRI scans were acquired at each visit using the previously described methods.⁷ All subjects were scanned with the same scanning protocol on 2 different 3 Tesla Achieva Medical Scanners from Philips (Philips, Australia). More information on acquisition protocols can be found in Table S1. The King's stages were derived from the ALSFRS-R.¹⁴ This study was approved by the Medical Ethical Committee of the UMC Utrecht and written informed consent was obtained from all participants.

Data Pre-Processing

A schematic overview of the methodology can be found in Figure 1. T1 images were processed using Freesurfer version 6.0. This pre-processing software parcellates the brain into gray and white matter structures and measures cortical thickness at around 150,000 vertices per hemisphere. All scans were resampled to a common space, allowing vertex-wise comparisons of cortical thickness. Values were smoothed using a full width half maximum at 10 mm.

To ensure clustering was performed only on disease-specific brain characteristics and not on age, sex, or other non-disease-specific predictors of cortical thickness, these variables were regressed out in 2 steps. First, a linear model was fitted at each vertex using scans of control subjects, with age and sex as covariables. This model was used to calculate residuals for all subjects. Second, a principal component analysis was performed on these residuals within control subjects to capture disease-unrelated brain variation in the general population. After analyzing the scree plot, 2 principal components were used to fit a linear model within control subjects, using the residuals calculated in the first model. This second model was subsequently used to calculate new residuals for patients with ALS. Residuals were calculated and Z-transformed, creating atrophy maps for each patient independent of age, sex, or naturally occurring brain variation.

DTI images were acquired using methods described in earlier work.⁷ Connectomes were created by reconstructing white matter tracts between 68 cortical regions (Desikan-Killiany atlas)¹⁵ and 15 subcortical structures, using fiber assignment for continuous tracking (FACT).¹⁶ Detailed methods can be found in previous publications.¹⁷ Average weighted fractional anisotropy was calculated for each white matter tract. During the

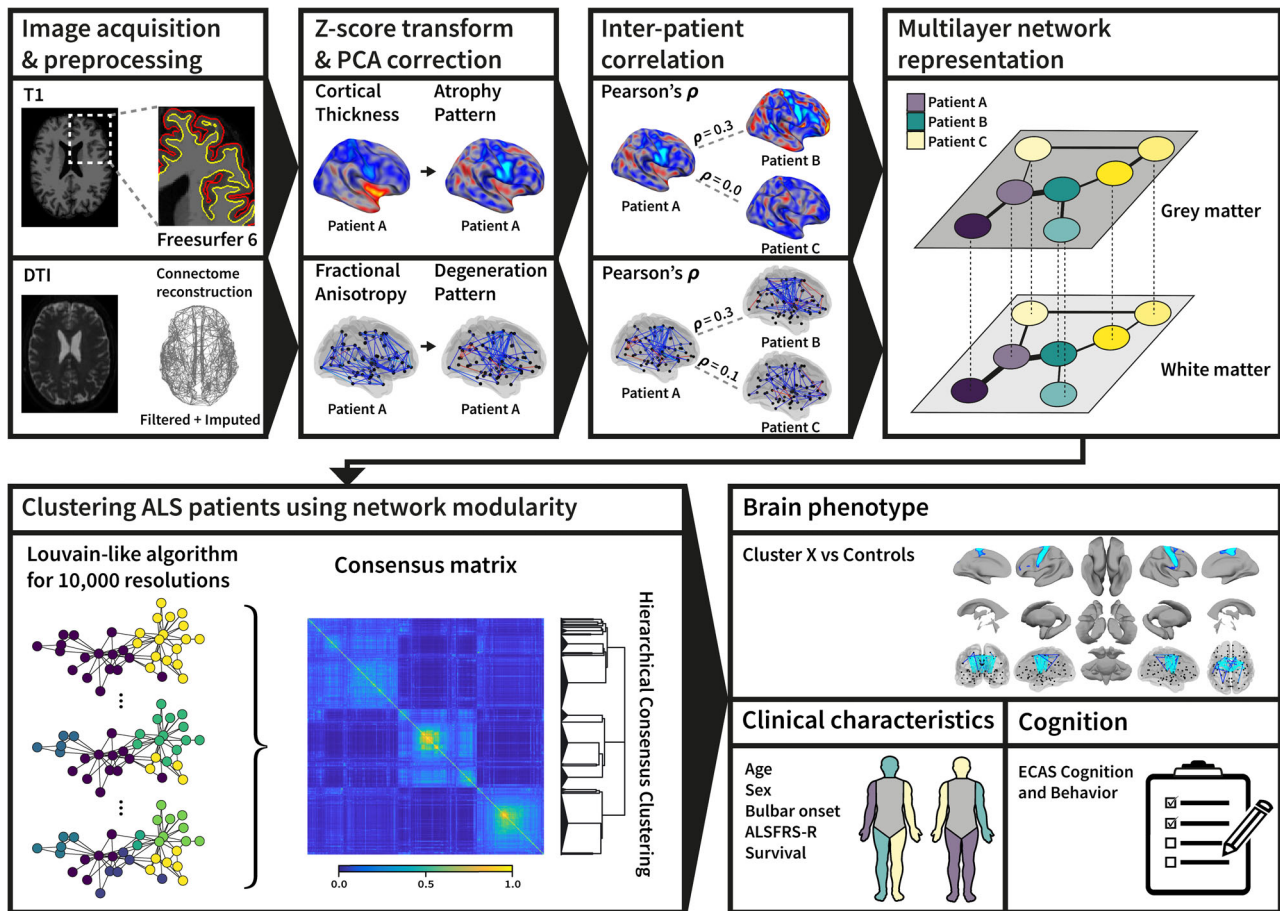


FIGURE 1: Overview of methodology. T1-weighted brain images are parcellated for each subject and resampled to a common space. Diffusion tensor imaging (DTI) brain images are used to reconstruct white matter tracts connecting the 68 regions of the Desikan–Killiany atlas and 15 subcortical structures and brainstem (“connectome”). Cortical thickness and fractional anisotropy are calculated and corrected for age, sex, and 2 principal components (reflecting disease-unrelated brain variation) using a linear model in healthy controls. This model is applied to patients and residuals are calculated and Z-transformed. Between each possible pair of patients with ALS, the resulting Z-score maps are compared using Pearson’s ρ for both T1 and DTI data separately. The comparisons between all patients can be captured in a multilayer network representation in which Pearson’s ρ represents the connectivity between patients. Subsequently, a Louvain-like algorithm is performed for 10,000 resolutions, after which hierarchical consensus clustering identifies subgroups of patients that display higher degrees of similarity in terms of neurodegeneration patterns. ALS = amyotrophic lateral sclerosis; ALSFRS-R = revised amyotrophic lateral sclerosis functional rating scale; DTI = diffusion tensor imaging; ECAS = Edinburgh cognitive and behavioral ALS screen.

reconstruction of individual patient connectomes using FACT, connections that are not present in the brain may erroneously be reconstructed, whereas reconstruction of true connections may be unsuccessful. Due to intersubject brain heterogeneity, this pattern may vary from person to person. To balance the inclusion of false positive and false negative connections for analysis, we selected connections for analysis based on a recommended threshold of 70% missing data in control subjects.¹⁸ This process of connectome reconstruction inherently leads to missing data for every subject, which may be problematic when performing interpatient comparisons (eg, Pearson’s ρ for one pair of patients may be based on 150 connections, but on 500+ connections for another pair of patients). To keep interpatient comparisons as consistent as possible, we performed multiple imputations on the missing fractional anisotropy using predictive mean matching from the “mice” package in R, resulting in 100 imputed DTI datasets.¹⁹ For each

connection, age, sex, and patient/control status were included as predictors for imputation, along with fractional anisotropy values of multiple other connections, provided the connections correlated with a minimal Pearson’s ρ of 0.25, and had a minimum proportion of usable cases of 0.90. Similar to T1 data, pooled linear models for age and sex were fitted for each white matter tract using the reconstructed connectomes of control subjects. In each imputed dataset, the residuals from these linear models were used to fit 2 principal components in control subjects to capture and regress out normal brain variation. The residuals were Z-transformed and used to create disease-specific white matter degeneration maps over the 100 imputed datasets.

Clustering Algorithm

For each modality (ie, both T1 and DTI data), the similarity between Z-transformed brain maps of each possible pair of

patients was calculated using Pearson's ρ for T1 data and pooled Pearson's ρ (using Rubin's rules) for DTI. The clustering algorithm used does not incorporate negative values. Therefore, negative values for ρ were set to zero, meaning that brain similarity was considered, but not dissimilarity. The resulting values for ρ were gathered in two (one for T1 and one for DTI data) 488 by 488 similarity matrices, which were fused in a multilayer network by creating an inpatient connection (ie, connecting T1 and DTI matrices with a weight of one for each individual) to ensure that a single individual would not be assigned to 2 different clusters (more information is given in Table S2).

To identify clusters of distinct brain phenotypes, we used the method described by Jeub et al.²⁰ A Louvain-like algorithm was applied to identify modules within the network, which comprise patients who share similar patterns of brain degeneration. The process is repeated for 10,000 samples of the resolution parameter, collecting information over different clustering sizes in a probabilistic manner. The resulting 10,000 subdivisions are fused into one 488 by 488 consensus matrix, each value representing the frequency with which 2 patients are clustered in the same module. A hierarchical consensus clustering procedure is used to find significant partitions within the consensus matrix using a permutation model. This algorithm is iteratively repeated for each subdivision, resulting in a hierarchical structure of partitions. This network-based clustering method allowed us to cluster on similarity in high dimensional data, without the need for prior input (ie, number of clusters or resolution parameter), hence providing insight into hierarchical structures within the data. In this study, we will focus primarily on the upper level of the hierarchical structure (ie, the first subdivision). Cluster consensus was calculated for each cluster at this level by computing the mean consensus value for each pair of patients within a cluster. Subclusters of the second level of the hierarchical clustering were analyzed to visualize the level of heterogeneity at this level.

Visualizing Cluster Characteristics

Characteristics of each cluster were explored by comparing the gray and white matter of patients in each cluster directly to all 338 control subjects. Linear models were used for cortical thickness using age and sex as covariates. Although subcortical volumes (19 subcortical structures and 6 ventricular) and cerebellar subfields (28 regions) were not included in the clustering algorithm due to the low dimensionality of the data, these data were analyzed for each cluster with linear models, using age, sex, and estimated total intracranial volume as covariates. Cerebellar subfields were measured after segmentation of T1-weighted images using automatic cerebellum anatomical parcellation using U-Net with locally constrained optimization (ACAPULCO).²¹ Fractional anisotropy was analyzed using pooled linear models with covariates for age and sex.

To correct for multiple testing, we used FMRIB Software Library (FSL) Permutation Analysis of Linear Models (PALM) together with threshold-free cluster enhancement (TFCE) for cortical thickness analyses.^{22,23} Bonferroni corrections were performed on fractional anisotropy analyses and subcortical

structure analyses. The p values <0.05 (after correction for multiple testing) were considered significant for all analyses in this study.

Clinical and Cognitive Associations

Clinical characteristics were collected at the time of diagnosis or as soon as possible thereafter. We determined site of symptom onset, age at symptom onset, the presence of FTD, and *C9orf72* and *UNC13A* genotype. Disease progression rates were calculated using the slope of the ALSFRS-R, defined as (48 ALSFRS-R score)/months since onset. Survival status was obtained from municipal records. Differences between clusters were analyzed using linear and logistic regression models. An additive genetic model was used to analyze *UNC13A*. Due to their non-normal distribution, the variables for disease duration, ALSFRS-R score, and ALSFRS-R slope were analyzed using the Mann-Whitney U test. To assess clinical signs of lower and upper motor neuron (UMN) involvement, patients underwent neurological examinations at each study visit, which were scored according to the Devine scoring method.²⁴⁻²⁶ Total UMN and lower motor neuron (LMN) sum scores were analyzed and compared between clusters using linear regression.

ECAS data on cognitive status and behavioral abnormalities were used to analyze differences in cognitive and behavioral impairment between the resulting clusters and between clusters and control subjects. A complete case analysis of ECAS data was performed. ECAS scores were classified as normal or abnormal using normative data (based on age, sex, and education) that had been derived from the Dutch population in an earlier study.¹³ The Strong criteria for ALS with cognitive impairment (ALS-ci), ALS with behavioral impairment (ALS-bi), and ALS with frontotemporal dementia (ALS-FTD) were derived from ECAS data.²⁷ The frontal assessment battery (FAB),²⁸ administered at diagnosis from 2011 onward, was included in the analysis. Scores <13 were considered abnormal. The p values were calculated using logistic regression, using impairment of cognitive or behavioral measures as an independent variable and cluster as a dependent variable. The ALS-FTD Questionnaire (ALS-FTD-Q) for behavioral symptoms was filled in by proxies and patients were categorized as having none, mild, or severe behavioral impairment according to previously defined cutoffs.²⁹

Longitudinal Analysis

Follow-up scans were processed identically to the baseline scans. A multilayer network was constructed similarly to the cross-sectional data, without including prior information about the subject to whom the scans belonged, thus treating each scan separately. The same clustering algorithm was then applied to the network. Of the resulting clusters, the cortical thickness and fractional anisotropy were compared with controls using linear mixed models, corrected for age and sex, while also including a random intercept for each patient. For each patient, we analyzed whether there were transitions between clusters over the course of their follow-up. The longitudinal data were analyzed for transitional trends, which could potentially represent transitions in disease stages, rather than different disease subtypes.

Sensitivity Analysis

To account for possible biases being introduced due to scanner effects, we repeated the clustering analysis adding the scanner as a covariable in the first model (in addition to age and sex). The brain phenotypes of the resulting clusters were subsequently visualized using the method described above.

Results

Demographics

Demographics are shown in Table 1. Patients with ALS (n = 488) and controls (n = 338) were well matched for age and sex. We aimed to include patients early in the course of disease: the median disease duration at the first MRI scan was 14.5 months (interquartile range [IQR] = 10.0–22.6 months).

Clustering Results

The clustering algorithm identified 3 main clusters of 187, 163, and 138 patients based on neurodegeneration patterns that are independent of naturally occurring variation. The main clusters showed a mean cluster consensus of 22.0%, 26.4%, and 30.6%, respectively, compared to a mean inter-cluster consensus of 7.8%. An overview of the consensus matrix and clustering dendrogram, along with the brain phenotypes, can be found in Figure 2.

Brain Phenotype

The largest main cluster (n = 187) can be described as a pure motor phenotype (pure motor cluster [PM]), characterized by isolated cortical thinning at the precentral gyrus, together with lower fractional anisotropy located at the corticospinal tract and surrounding white matter tracts when compared with controls. (Data on white matter tracts can be found in Table S3.) There was no volume loss of subcortical structures or ventricular enlargement. Cerebellar subfield analysis did not reveal any volume loss (Table 2).

The second main cluster (n = 163) showed cortical thinning of the entire frontal cortex, including the precentral gyrus, prefrontal, and orbitofrontal cortices, as well as anterior temporal lobe involvement and predominantly left occipitoparietal thinning. White matter degeneration was concordant with frontotemporal atrophy, shown by an impaired white matter network connecting orbitofrontal and anterior temporal regions. Analyses of subcortical structures revealed a significantly smaller amygdala, hippocampus, and basal ganglia in both hemispheres, in addition to enlargement of both the lateral ventricle temporal horns of the third ventricle and fourth ventricles. In the cerebellum, white matter volumes were lower in the left hemisphere compared to controls, but cerebellar gray matter volumes did not differ from controls.

Cerebellar subfield analysis did not show any volume loss. This cluster will be referred to as the frontotemporal cluster (FT) in the remainder of this paper.

The third main cluster (n = 138) is characterized by cortical thinning along the posterior cingulate and isthmus cingulate regions, together with thinning in the temporal, occipital, and medial frontal regions. Motor and premotor regions are also affected, consistent with the diagnosis of ALS. Compared to the FT cluster, orbitofrontal regions were spared. White matter analyses showed degeneration of tracts connected with the posterior cingulate cortex and the superior parietal cortex. Analyses of the subcortical structures revealed involvement of bilateral thalamus, lentiform nucleus, hippocampus, and cerebellum, but sparing of the caudate nucleus and amygdala. Moreover, cingulate-parietal-temporal cluster (CPT) showed ventricular enlargement of both lateral ventricles and temporal horns, as well as the third ventricle. Cerebellar subfield analyses showed cerebellar atrophy predominantly involving the corpus medullare, lobules V and VIIB right, and bilateral IX. In the remainder of this paper, we will refer to this cluster as the CPT.

Inter-cluster comparisons are illustrated in Figure 3. A closer look at FT versus CPT comparisons revealed significantly greater involvement of the posterior cingulate cortex and the parietal white matter in CPT, in addition to larger lateral ventricle volumes. FT showed more severe involvement of orbitofrontal and anterior temporal gray and white matter, in addition to more severe atrophy of the caudate nucleus, amygdala, and parietal cortex.

Using our hierarchical clustering algorithm, the 3 main clusters of brain phenotypes can be further subdivided. There were 2 subclusters per main cluster: a smaller subcluster (PM-A: n = 35, FT-A: n = 28, and CPT-A: n = 13) and a larger subcluster (PM-B: n = 152, FT-B: n = 135, and CPT-B: n = 125). Neurodegeneration patterns of the larger subclusters were in line with those of the main clusters. Although the sample size differences in these subclusters require careful interpretation, PM-A showed right frontal cortical thinning in addition to precentral and corticospinal neurodegeneration, FT-A showed pure right frontal lobe thinning, and CPT-A showed parietal white matter involvement with cortical thinning limited to the precentral gyrus. A total of 26 clusters were found at the finest partition. These subclusters are considerably smaller; therefore, reliable characterization is more challenging.

Clinical Characteristics

Clinical characteristics for each cluster are described in Table 3. Patients in the PM group were predominantly men (73.3%), younger at disease onset

TABLE 1. Cohort Characteristics

Variable	ALS	Controls	Missing data, %
<i>n</i>	488	338	
Sex, M	324 (66.4)	229 (67.8)	0
Age at onset, yr	60.5 (52.6–66.6)		0.8
Age at first MRI, yr	62.3 (54.0–68.2)	62.7 (55.2–68.8)	0
Disease duration at inclusion, mo	14.5 (10.0–22.6)	–	0.8
Total number of scans per subject, 1/2/3/4	213/128/57/90	338/0/0/0	
Bulbar onset	115 (23.9)	–	1.2
ALS-FTD clinical diagnosis	11 (3.1)	–	26.2
Survival, mo, median (95% CI)	40.4 (37.9–44.2)	–	0.8
<i>C9orf72</i> repeat expansions	42 (9.0)	–	4.3
<i>UNC13A</i> genotype			19.9
A/A	162 (41.4)	–	
A/C	175 (44.8)	–	
C/C	54 (13.8)	–	
<i>UNC13A</i> MAF	0.36	–	19.9
King's stage, 1/2/3/4a/4b ^a	157/160/156/3/6		3.9
UMN sum score	7.0 (5.0–10.0)	–	37.5
LMN sum score	8.0 (6.0–10.0)	–	35.9
ALSFRS-R score	40.0 (36.0–43.0)	–	4.7
ALSFRS-R slope ^b	0.52 (0.29–0.85)	–	5.3
ECAS administered	272 (55.7)	142 (42.0)	
Abnormal ALS-specific score ^c	35 (12.9)	8 (5.7)	49.8
Abnormal nonspecific score ^c	17 (6.3)	2 (1.4)	49.8
Abnormal total score ^c	34 (12.5)	8 (5.7)	49.8
FAB administered	337 (69.0)	146 (43.2)	
FAB abnormal, <13	25 (7.4)	4 (2.7)	41.5
ALS-FTD-Q administered	233 (47.7)	–	
Mild to severe behavioral changes, >22	38 (16.3)	–	52.3
Severe behavioral changes, >29	20 (8.6)	–	52.3

Values are median (IQR) for continuous data and count (%) for categorical data unless otherwise specified. No significant differences were found between patients with ALS and controls.

^aDerived from ALSFRS-R questionnaires.

^bDisplayed in ALSFRS-R points decrease per month since symptom onset.

^cECAS data abnormal scores are derived from Dutch normative data in a previous study.¹³

95% CI = 95% confidence interval; ALS = amyotrophic lateral sclerosis; ALSFRS-R = revised amyotrophic lateral sclerosis functional rating scale; ALS-FTD-Q = Amyotrophic Lateral Sclerosis Frontotemporal Dementia Questionnaire; ECAS = Edinburgh cognitive and behavioral amyotrophic lateral sclerosis screen; FAB = frontal assessment battery; FTD = frontotemporal dementia; IQR = interquartile range; LMN = lower motor neuron; MAF = minor allele frequency; MRI = magnetic resonance imaging; UMN = upper motor neuron.

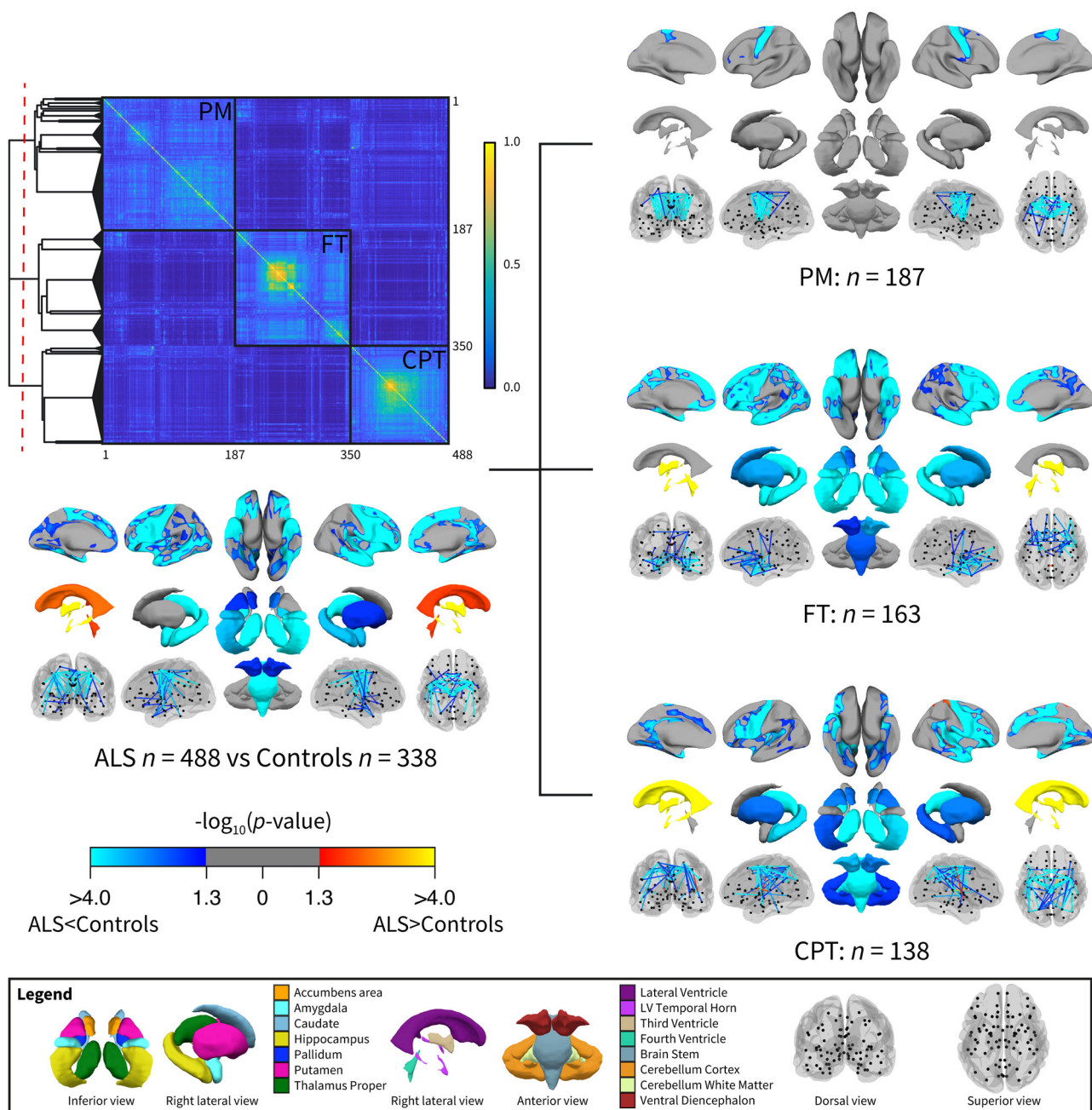


FIGURE 2: Clustering matrix and phenotype of 3 main clusters compared to controls. Consensus matrix and neurodegeneration patterns for the 3 resulting ALS clusters: PM (pure motor), FT (frontotemporal), and CPT (cingulate-parietal-temporal). The consensus matrix is the result of the probabilistic clustering algorithm. Both columns and rows represent individual patients. Colors represent the frequency with which a pair of patients were clustered together over the 10,000 clustering iterations. The dendrogram on the left of the consensus matrix shows the outcomes of the hierarchical clustering. Results are displayed for the first level in the clustering hierarchy (red dashed line). For both gray matter (cortical thickness and subcortical volumes) and white matter parameters (fractional anisotropy) of each cluster, group comparisons were performed with control subjects ($n = 338$), using linear models with age and sex (and estimated total intracranial volume for volumetric analyses) as covariables. Resulting p values were corrected for multiple comparisons using permutations and TFCE for cortical thickness analyses and were Bonferroni corrected for subcortical volumes and fractional anisotropy analyses. Neurodegeneration patterns of cortex, deep gray matter, ventricles, brain stem, cerebellum, and white matter are displayed for each cluster. ALS = amyotrophic lateral sclerosis; CPT = cingulate-parietal-temporal cluster; FT = frontotemporal cluster; PM = pure motor cluster; TFCE = threshold-free cluster enhancement; LV = lateral vent.

(median = 56.5 years), and the frequency of bulbar symptom onset was relatively low (13.0%). The FT cluster comprised relatively more women (56.4% men,

$p = 0.001$ vs PM) and patients were older at disease onset (median = 62.1 years, $p < 0.001$ vs PM), with a higher percentage of bulbar onset (29.8%, $p < 0.001$ vs PM). As

TABLE 2. Volumes of Cerebellar Subfields for Each Cluster

Subfield	Cluster				Corrected p^a CPT vs controls
	Controls	PM	FT	CPT	
Corpus medullare	13.28 (13.14–13.43)	13.46 (13.26–13.67)	13.05 (12.84–13.26)	12.73 (12.51–12.96)	0.006
Left I–III	0.87 (0.85–0.89)	0.84 (0.81–0.86)	0.86 (0.84–0.89)	0.86 (0.83–0.89)	NS
Left IV	3.41 (3.35–3.46)	3.41 (3.33–3.49)	3.51 (3.43–3.59)	3.35 (3.26–3.44)	NS
Left V	3.21 (3.17–3.26)	3.16 (3.09–3.22)	3.23 (3.17–3.30)	3.08 (3.01–3.16)	0.067
Left VI	9.16 (9.03–9.29)	9.17 (8.99–9.35)	8.89 (8.70–9.07)	8.93 (8.72–9.13)	NS
Left VIIA–Crus I	12.93 (12.75–13.11)	13.05 (12.8–13.30)	12.58 (12.32–12.84)	12.49 (12.21–12.77)	NS
Left VIIA–Crus II	7.63 (7.50–7.76)	7.62 (7.44–7.79)	7.66 (7.49–7.84)	7.60 (7.40–7.79)	NS
Left VIIB	5.92 (5.83–6.02)	5.81 (5.67–5.94)	5.83 (5.70–5.97)	5.68 (5.53–5.83)	NS
Left VIIIA	5.48 (5.37–5.59)	5.49 (5.34–5.65)	5.52 (5.36–5.67)	5.34 (5.17–5.51)	NS
Left VIIIB	3.28 (3.21–3.34)	3.31 (3.22–3.40)	3.26 (3.17–3.35)	3.09 (2.99–3.19)	0.094
Left IX	3.24 (3.18–3.31)	3.21 (3.13–3.30)	3.21 (3.12–3.30)	3.03 (2.94–3.13)	0.022
Left X	0.49 (0.48–0.50)	0.49 (0.48–0.50)	0.49 (0.48–0.50)	0.47 (0.46–0.49)	NS
Right I–III	0.88 (0.86–0.90)	0.84 (0.82–0.87)	0.88 (0.85–0.90)	0.91 (0.88–0.93)	NS
Right IV	3.52 (3.46–3.57)	3.49 (3.41–3.57)	3.53 (3.45–3.61)	3.44 (3.35–3.53)	NS
Right V	3.43 (3.38–3.48)	3.39 (3.32–3.45)	3.38 (3.32–3.45)	3.27 (3.19–3.34)	0.027
Right VI	8.90 (8.78–9.02)	8.90 (8.73–9.07)	8.63 (8.45–8.80)	8.67 (8.48–8.86)	NS
Right VIIA–Crus I	12.99 (12.81–13.17)	13.14 (12.89–13.39)	12.77 (12.52–13.03)	12.70 (12.42–12.98)	NS
Right VIIA–Crus II	8.21 (8.07–8.36)	8.13 (7.94–8.33)	8.21 (8.01–8.41)	8.27 (8.05–8.49)	NS
Right VIIB	5.96 (5.86–6.05)	5.84 (5.70–5.97)	5.86 (5.73–6.00)	5.67 (5.52–5.82)	0.045
Right VIIIA	4.50 (4.41–4.59)	4.51 (4.39–4.64)	4.65 (4.53–4.78)	4.38 (4.24–4.52)	NS
Right VIIIB	3.41 (3.35–3.48)	3.49 (3.41–3.58)	3.42 (3.34–3.51)	3.22 (3.13–3.32)	0.051
Right IX	3.13 (3.06–3.19)	3.13 (3.04–3.22)	3.07 (2.99–3.16)	2.92 (2.83–3.02)	0.018
Right X	0.49 (0.48–0.50)	0.49 (0.48–0.51)	0.49 (0.48–0.50)	0.48 (0.47–0.49)	NS
Vermis VI	1.57 (1.54–1.59)	1.56 (1.53–1.59)	1.55 (1.52–1.58)	1.53 (1.50–1.56)	NS
Vermis VII	1.00 (0.99–1.02)	1.01 (0.98–1.03)	0.98 (0.96–1.01)	1.00 (0.97–1.02)	NS
Vermis VIII	2.05 (2.02–2.08)	2.06 (2.02–2.10)	2.05 (2.01–2.10)	2.02 (1.97–2.06)	NS
Vermis IX	1.02 (1.01–1.04)	1.01 (0.99–1.04)	0.99 (0.97–1.01)	1.01 (0.98–1.03)	NS
Vermis X	0.34 (0.34–0.35)	0.34 (0.33–0.34)	0.33 (0.32–0.34)	0.33 (0.33–0.34)	NS

Estimated marginal means and p -values derived from a linear model, using age, sex and estimated intracranial volume as covariates. p -values are corrected using Bonferroni's method. Volumes are given in cm^3 (95% confidence interval).

^aNo significant differences were found for PM versus controls and FT versus controls.

CPT = cingulate-parietal-temporal cluster; FT = frontotemporal cluster; NS = not significant and p value >0.10 ; PM = pure motor cluster.

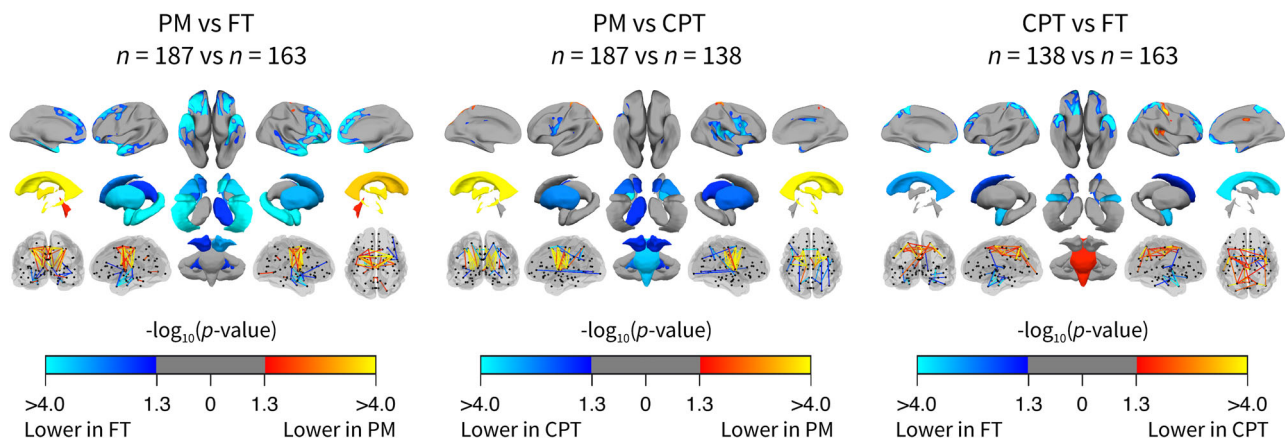


FIGURE 3: Inter-cluster neurodegeneration comparison. The p value maps of whole-brain inter-cluster comparison of neurodegeneration patterns. Cortical thickness and fractional anisotropy are analyzed using a linear model, using age and sex as covariables. Subcortical volumes are analyzed using the same model containing estimated total intracranial volume as an extra covariate. Resulting p values were corrected for multiple comparisons using permutations and TFCE for cortical thickness analyses and were Bonferroni corrected for subcortical volumes and fractional anisotropy analyses. Neurodegeneration patterns of cortex, deep gray matter, ventricles, brain stem, cerebellum, and white matter are displayed for each cluster. CPT = cingulate-parietal-temporal cluster; FT = frontotemporal cluster; PM = pure motor cluster; TFCE = threshold-free cluster enhancement.

expected, most of the patients with a clinical diagnosis of FTD were assigned to the FT cluster (8 [6.6%] vs PM: 1 [0.8%], $p = 0.036$; vs CPT: 2 [1.9%], $p = 0.10$). Distinct from FT, the CPT cluster was predominantly men (68.8%, $p = 0.028$ vs FT), and distinct from PM, had an older age at onset (median = 62.2 years, $p < 0.001$ vs PM) and more frequent bulbar onset of symptoms (31.4%, $p < 0.001$ vs PM). No differences were found in survival rates since symptom onset, nor was there a difference between disease duration. Analysis of clinical stages did not reveal significant differences; however, a nonsignificant trend ($p = 0.097$) was detected, in that CPT appeared to have a higher King's stage compared to FT, but not compared to PM. UMN sum scores were lower in FT ($p = 0.004$ vs PM and $p = 0.009$ vs CPT), indicating less UMN symptoms, whereas LMN scores did not differ. ALSFRS-R scores on MRI were higher in the FT cluster ($p = 0.003$ vs PM, $p = 0.004$ vs CPT). *C9orf72* mutation and *UNC13A* SNP were not associated with the different clusters.

Cognition and Behavior

For 272 patients and 171 controls included after 2015, an ECAS was administered at time of the first MRI scan. In 166 patients, the ECAS behavioral screen was administered to proxies. ECAS data were available for 117 (62.6%) patients in the PM group, 93 (57.0%) patients in the FT group, 62 (44.9%) patients in the CPT group, and 142 (42.0%) controls. Cognitive abnormalities according to the ECAS are presented in Figure 4. The PM group did not differ from the control subjects on any of the domains. For FT, there were significantly higher

frequencies of patients with cognitive impairment in language (20.4% vs controls 7.8%, $p = 0.006$), executive function (13.0% vs controls 3.5%, $p = 0.011$), and memory domains (16.5% vs controls 6.3%, $p = 0.016$), when compared with control subjects. For FT, higher rates of abnormal sum scores were also found on the ALS-specific sum score (15.4% vs controls 5.7%, $p = 0.018$), nonspecific score (8.8% vs controls 1.4%, $p = 0.017$), and total score (14.4% vs controls 5.7%, $p = 0.029$). Compared with controls, CPT also showed significantly more patients with abnormal ALS-specific sum scores (15.0% vs controls 5.7%, $p = 0.037$), nonspecific sum score (8.2% vs controls 1.4%, $p = 0.031$), and total score (15.0% vs controls 5.7%, $p = 0.037$). For CPT, this lower ALS-specific sum score was mainly driven by differences in language (17.7% vs controls 7.8%, $p = 0.041$) and executive domains (13.3% vs controls 3.5%, $p = 0.016$).

Between-cluster comparisons showed a difference between FT and PM in language (FT 20.4% vs PM 8.5%, $p = 0.016$) and memory domains (FT 16.5% vs PM 7.0%, $p = 0.036$). CPT showed significantly more patients who fulfilled the criteria for ALS-ci, compared to PM (CPT 40.3% vs PM 33.3%, $p = 0.028$). No other differences were found between FT and CPT or between CPT and PM. Behavioral questions from the ECAS and the criteria for ALS-bi and ALS-FTD derived from these were also compared between clusters, but yielded no significant findings. The FAB was administered in 337 (69.0%) patients and showed a significantly higher proportion of abnormal scoring patients in FT compared to PM (FT 11.9% vs PM 3.9%, $p = 0.027$), but this did not differ from CPT (FT 11.9% vs CPT 6.5%,

TABLE 3. Disease Characteristics Per Cluster

Variable	Cluster			<i>p</i>		
	PM	FT	CPT	PM vs FT	PM vs CPT	FT vs CPT
<i>n</i>	187	163	138			
Sex, M	137 (73.3)	92 (56.4)	95 (68.8)	0.001	NS	0.028
Age at onset, yr	56.5 (48.9–63.1)	62.1 (55.0–67.5)	62.2 (55.9–69.1)	<0.001	<0.001	NS
Age at MRI, yr	58.2 (50.4–64.9)	64.0 (56.3–69.0)	64.7 (57.7–70.9)	<0.001	<0.001	NS
Disease duration, mo	14.7 (9.8–22.4)	15.0 (10.1–22.1)	14.1 (10.3–24.3)	NS	NS	NS
Bulbar onset	24 (13.0)	48 (29.8)	43 (31.4)	<0.001	<0.001	NS
ALS-FTD clinical diagnosis	1 (0.8)	8 (6.6)	2 (1.9)	0.036	NS	0.10
Survival, mo, median (95% CI) ^a	45.6 (39.6–49.1)	39.0 (32.7–42.9)	39.3 (32.7–51.1)	NS	NS	NS
<i>C9orf72</i> repeat expansions	15 (8.6)	16 (10.2)	11 (8.1)	NS	NS	NS
<i>UNC13A</i> genotype				NS	NS	NS
<i>A/A</i>	63 (43.4)	54 (41.5)	45 (38.8)			
<i>A/C</i>	63 (43.4)	63 (48.5)	49 (42.2)			
<i>C/C</i>	19 (13.1)	13 (10.0)	22 (19.0)			
<i>UNC13A</i> MAF	0.35 (0.35)	0.34 (0.32)	0.40 (0.37)			
King's stage, 1/2/3/4a/4b ^b	54/71/56/1/3	58/55/45/2/0	45/34/55/0/3	NS	NS	0.097
UMN sum score	8.0 (5.0–10.0)	6.0 (4.0–8.0)	7.0 (5.0–10.5)	0.004	NS	0.009
LMN sum score	8.0 (6.0–10.0)	7.0 (6.0–10.0)	8.0 (6.0–11.0)	NS	NS	NS
ALSFRS-R score	39.0 (36.0–42.0)	41.0 (38.0–43.0)	39.0 (34.0–42.8)	0.003	NS	0.004
ALSFRS-R slope ^c	0.54 (0.33–0.90)	0.47 (0.27–0.75)	0.50 (0.27–0.86)	0.066	NS	NS
ECAS administered at MRI	117 (62.6)	93 (57.0)	62 (44.9)			
Abnormal ALS-specific score ^d	12 (10.4)	14 (15.4)	9 (15.0)	NS	NS	NS
Abnormal nonspecific score ^d	4 (3.5)	8 (8.8)	5 (8.2)	NS	NS	NS
Abnormal total score ^d	12 (10.5)	13 (14.4)	9 (15.0)	NS	NS	NS
FAB administered	127 (67.9)	118 (72.4)	92 (66.7)			
FAB abnormal, <13	5 (3.9)	14 (11.9)	6 (6.5)	0.027	NS	NS
ALS-FTD-Q administered	100 (53.5)	80 (49.1)	53 (38.4)			
Mild to severe behavioral changes, >22	17 (17.0)	17 (21.2)	4 (7.5)	NS	NS	0.042
Severe behavioral changes, >29	8 (8.0)	9 (11.2)	3 (5.7)	NS	NS	NS

Values are median (IQR) for continuous data and count (%) for categorical data unless otherwise specified. The *p* values are computed using linear models for continuous variables and logistic models for categorical variables. Variables *UNC13A* and King's stage were treated as ordinal, the *p* values are calculated using the Cochran-Armitage trend test. The *p* values for disease duration, ALSFRS-R score, ALSFRS-R slope, and ALS-FTD-Q total score were calculated using Mann-Whitney *U* test.

^aThe *p* value is calculated using a Cox proportional hazard model corrected for the linear predictor of the ENCALS model.²

^bDerived from ALSFRS-R questionnaires.¹¹

^cDisplayed in ALSFRS-R points decrease per month since symptom onset.

^dECAS data abnormal scores are derived from Dutch normative data in a previous study.¹³

95% CI = 95% confidence interval; ALS = amyotrophic lateral sclerosis; ALSFRS-R = revised amyotrophic lateral sclerosis functional rating scale; ALS-FTD-Q = Amyotrophic Lateral Sclerosis Frontotemporal Dementia Questionnaire; CPT = cingulate-parietal-temporal cluster; ECAS = Edinburgh cognitive and behavioral amyotrophic lateral sclerosis screen; FAB = frontal assessment battery; FT = frontotemporal cluster; FTD = frontotemporal dementia; IQR = interquartile range; LMN = lower motor neuron; MAF = minor allele frequency; MRI = magnetic resonance imaging; NS = not significant and *p* value >0.10; PM = pure motor cluster; UMN = upper motor neuron.

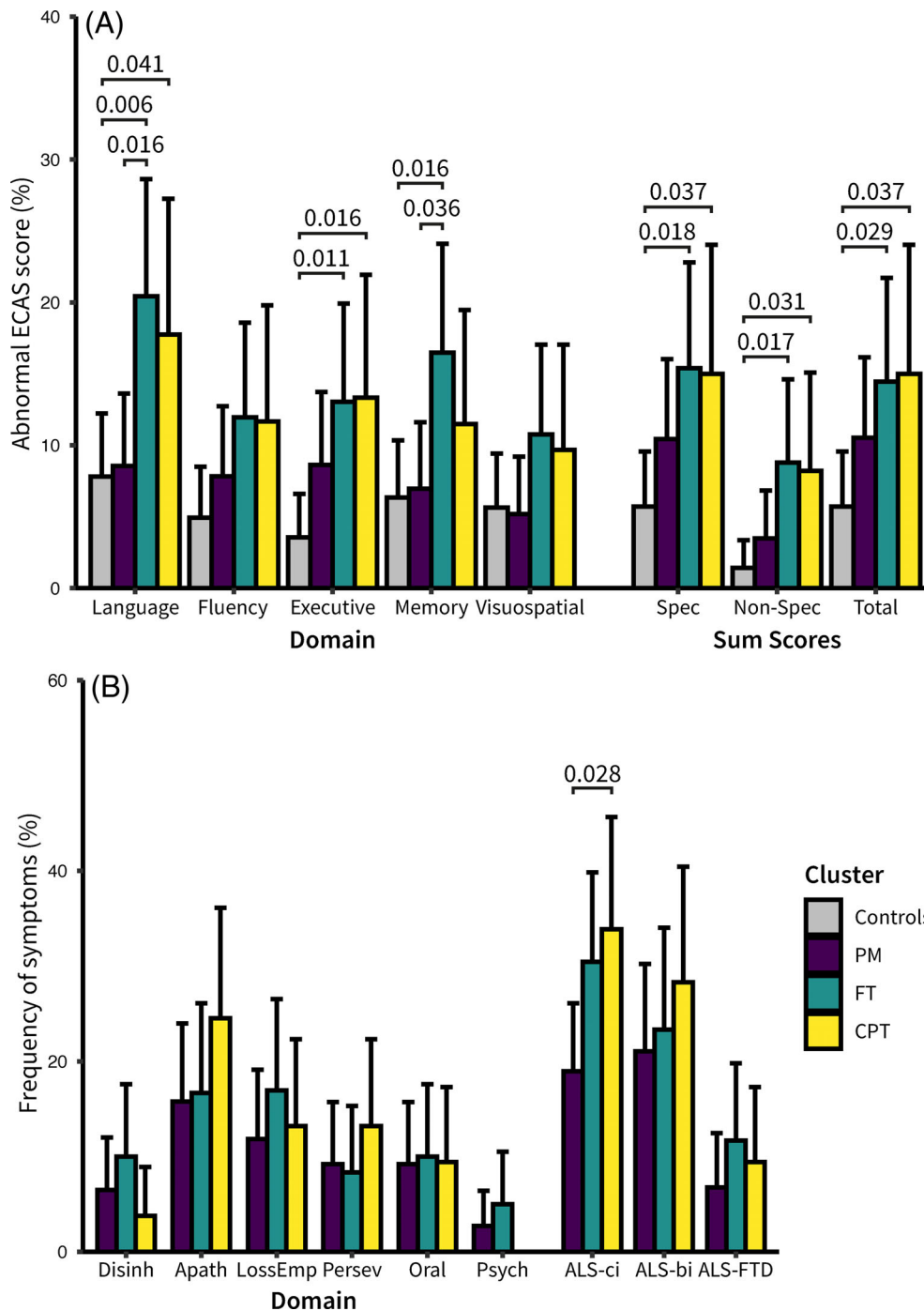


FIGURE 4: Cognitive profiles for each of the main clusters. (A) Proportions of abnormal cognition scores for the different cognitive domains on the ECAS. Cutoff scores are derived from Dutch normative data based on age, sex and education level.¹³ Error bars represent 95% confidence intervals. The p values are calculated using logistic regression models. Only significant p values are displayed above the data with brackets. **(B)** Frequency of behavioral symptoms derived from the proxy questionnaire of the ALS-bi = ALS with behavioral impairment; ALS-ci = ALS with cognitive impairment; and ALS-FTD = ALS with frontotemporal dementia. ALS = amyotrophic lateral sclerosis; Apath = apathy; CPT = cingulate-parietal-temporal cluster; Disinh = behavioral disinhibition; ECAS = Edinburgh cognitive and behavioral ALS screen; FT = frontotemporal cluster; LossEmp = loss of empathy/sympathy; NonSpec = ALS nonspecific sum score; Oral = hyperorality/altered eating behavior; Persev = perseverative/stereotyped behavior; PM = pure motor cluster; Psych = psychotic symptoms; Spec = ALS-specific sum score. [Color figure can be viewed at www.annalsofneurology.org]

$p = 0.20$). The ALS-FTD-Q was filled in by proxies of 233 (47.7%) patients. The FT cluster did show more patients with mild to severe behavioral symptoms than the

CPT cluster (FT 21.2% vs CPT 7.5%, $p = 0.042$), but this did not differ significantly from the PM group (FT 21.2% vs PM 17.0%, $p = 0.47$).

To analyze whether the neurodegeneration patterns of the FT and CPT clusters were not solely driven by specific subclusters of patients with cognitive impairment, we performed a sensitivity analysis in which patients with cognitive impairment were excluded from the FT and the CPT clusters. Cognitive impairment was defined as fulfilling the ALS-ci criteria using the ECAS or an abnormal score on the FAB. Using the available data, we identified 39 cognitively impaired and 108 cognitively normal patients in the FT group. In the CPT cluster there were 26 cognitively impaired and 89 cognitively healthy patients. Neurodegeneration patterns of cognitively

healthy patients were similar to the main cluster in both FT and CPT, showing that neurodegeneration patterns of the main clusters were not solely driven by a subcluster of cognitively impaired patients.

Longitudinal Analysis

Of the 488 participating patients, 213 (44%) had a single scan, 128 (26%) had a total of 2 scans, 57 (12%) had 3 scans, and 90 (18%) patients had 4 scans (total number of scans in patients = 1,000). The median time interval between scans was 4.2 (IQR = 3.4–5.7) months (described in more detail in Table S4). Clustering this

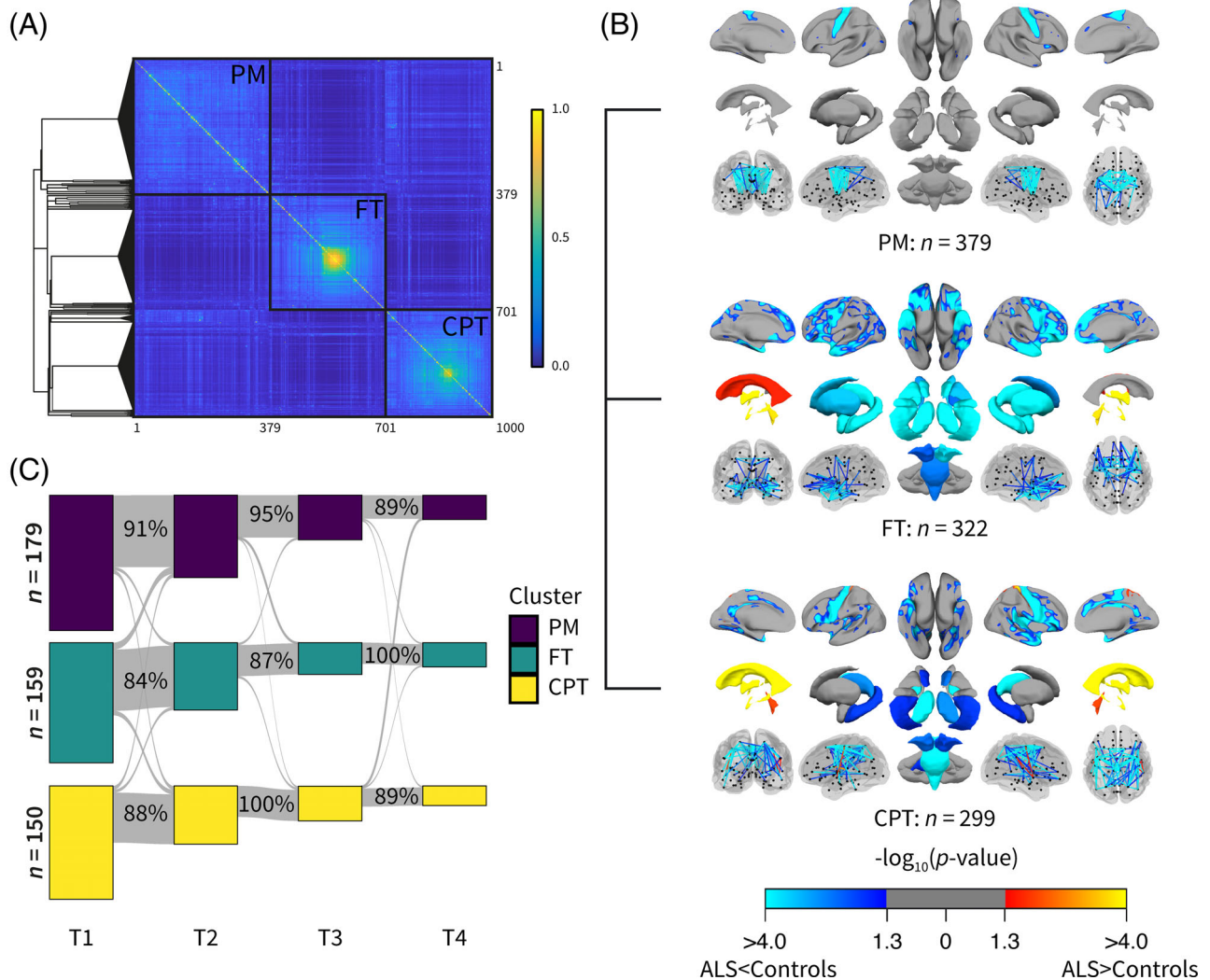


FIGURE 5: Longitudinal clustering results and cluster transitions. (A) Consensus matrix and (B) neurodegeneration patterns for the 3 clusters resulting from longitudinal data analysis. For both gray matter (cortical thickness and subcortical volumes) and white matter parameters (fractional anisotropy) of each cluster, group comparisons were performed with control subjects ($n = 338$, one scan only), using a linear mixed-effects model with age and sex (and estimated total intracranial volume for volumetric analyses) as covariables, accounting for between-subject variation using a random intercept. The p value maps were Bonferroni corrected for cortical thickness, subcortical volumes, and fractional anisotropy analyses. (C) Sankey diagram illustrating the transitions for each patient's follow-up scans. Columns represent different time points (T1 to T4), with bar sizes representing the total number of scans in each cluster at given time point. Gray flows represent transitions in patients' cluster assignments over the different timepoints. In 90.4% of the follow-up visits, patients remained in the same subgroup as their baseline visit. ALS = amyotrophic lateral sclerosis; CPT = cingulate-parietal-temporal cluster; FT = frontotemporal cluster; PM = pure motor cluster.

total of 1,000 scans resulted in 3 groups, whose brain phenotypes were identical to those found in the cross-sectional analysis (Fig 5A, B).

Patients were analyzed with regard to whether they were categorized in the same cluster over the different timepoints or whether they transitioned to another cluster over time. The transitions between the clusters over the different time points are depicted in a Sankey plot (Fig 5C). (Mean follow-up times and transition matrices can be found in Table S4). Of the 512 total follow-up scans, 463 (90.4%) were assigned to the same cluster as the baseline scan ($n = 488$) of the same patient. There were no between-cluster transitions that occurred remarkably more frequently, indicating that transitions observed are more likely caused by noise, rather than progression through possible stages.

Sensitivity Analysis

Analysis of scanner effects revealed that 290 patients and 152 controls were scanned using scanner A, and 198 patients and 186 controls were scanned on scanner B. Individual neurodegeneration maps were reconstructed by calculating Z -scores using an MRI scanner as a covariable in addition to age and sex. The repeated clustering analysis resulted in 3 main subgroups of 178, 159, and 151 patients. The resulting phenotypes were consistent with the main clustering analysis, and similarly showed characteristics of PM, FT, and CPT, respectively (Fig S1).

Discussion

By using a large multimodal neuroimaging dataset of, in total, 1,338 MRI scans from 488 clinically well-characterized patients with ALS and 338 control subjects, in combination with a probabilistic data-driven approach, we were able to identify 3 distinct subtypes of ALS, which can be described as a pure motor, a frontotemporal, and a cingulate-parietal-temporal variant of ALS. The large sample size allows the use of a network-based probabilistic clustering algorithm, which clusters according to neurodegeneration pattern similarity rather than severity and does not require prior assumptions to be made. The resulting neuroimaging subtypes are associated with distinct clinical features and congruent with cognitive function. Longitudinal analysis replicates cross-sectional clustering and reveals that patients usually remain in the same cluster over time, providing evidence for distinct subtypes of ALS rather than progressing disease stages. This finding challenges the hypothesis of the ALS-FTD spectrum being a linear spectrum of varying disease severity and shows that extra-motor neurodegeneration frequently occurs in patterns outside frontotemporal degeneration.

The discovery of the CPT subtype—characterized by cingulate, parietal, temporal, and cerebellar involvement—is novel in the field of ALS. Individual features of this subtype have been reported separately in previous, smaller, ALS neuroimaging studies: involvement of the cingulum has been reported, often related to cognitive impairment^{8,30–33}; decreased parietal white matter integrity has been reported, specifically seen in patients with behavioral impairment^{8,34}; furthermore, involvement of the cerebellum has been described in ALS by neuroimaging and histological studies.^{35–38} In our clustering approach involving over 1,000 MRI scans, we were able to identify a more comprehensive, separate, neuroimaging phenotype. As the CPT subtype comprises a smaller, yet significant, proportion of our neuroimaging cohort (138/488 patients, 28%), without sufficient stratification, different aspects of the phenotype would easily be diluted in studies with smaller sample sizes. A neuroimaging-based stratification of study populations could potentially provide new insights for researching other disease aspects of ALS.

Our cerebellar subfield analysis of CPT partially overlaps with an earlier meta-analysis showing similar focal upper lobule involvement (lobule V) and lower lobule involvement (VIIIb and IX), but not showing involvement of the Crus.³⁹ These regions are thought to be associated with somatomotor function and default mode network, which could be in line with the cerebral degeneration pattern found in CPT.^{40,41}

Despite significant differences in neurodegeneration patterns and clinical UMN presentation, we found that the CPT and FT subtypes are not distinguishable using the cognitive and behavioral screening tests that are frequently applied in clinical practice (ie, ECAS, ALSFTD-Q, and FAB). We do, however, note a trend in which the CPT cluster has a higher rate of apathy than the FT cluster, which could be linked to findings from a study linking parietal atrophy to apathy.⁴² Considering the significantly differing patterns of neurodegeneration in FT and CPT, it is unlikely that these patterns cause identical impairment of cognitive function. Because patients are stratified on patterns of neurodegeneration, rather than disease severity, it is possible that a substantial proportion of patients display mild, subclinical levels of FT or CPT type degeneration. Furthermore, the neuropsychological instruments that were used in this study are screeners designed to identify changes within the spectrum of FTD. Therefore, (subtle) cognitive deficits outside this spectrum may have been missed. We also note that the extent of extra-motor degeneration might not necessarily be related to severity of motor function, as the more widespread affected FT subgroup shows less motor impairment on

the ALS-FRS-R and King's stage than CPT. Future neuropsychological assessment studies might focus on uncovering a cognitive phenotype associated with the CPT neurodegenerative profile to differentiate more precisely clinical features of ALS subtypes.

Although FT is not distinguishable from CPT based on cognitive tests, most patients with clinically diagnosed ALS-FTD are assigned to the FT subgroup. Still, we see that 3 patients with a clinical diagnosis of ALS-FTD are assigned to either the PM or CPT subgroups. We explored their *Z*-score maps (adjusted for age and sex; Fig S2) and noticed that patients had relatively marked white matter degeneration, but no clear frontal and temporal gray matter involvement as seen in FT. Heterogeneity might indeed exist within patients with a clinical diagnosis of ALS-FTD. Studies in patients with behavioral variant FTD have revealed heterogeneous patterns of neurodegeneration,^{43,44} which may be related to heterogeneity found in clinical phenotypes of behavioral variant FTD.⁴⁵ Using current methods of ALS-FTD diagnosis, distinct neurodegeneration patterns might present as clinically overlapping syndromes.

Based on our study data, we were not able to find a genetic basis for these differences in neurodegeneration profiles. We found that patients with a *C9orf72* repeat expansion were not assigned to a single neurodegenerative pattern. Previous studies have reported a neurodegenerative signature associated with *C9orf72*, characterized by widespread cortical and subcortical degeneration, most severe in frontal and temporal brain lobes.^{46,47} Yet, little is known about the within-group heterogeneity that is present in patients with a *C9orf72*-mutation. In this study, we demonstrate that *C9orf72* carriers are not confined to a single neurodegenerative profile; this is to be expected, considering the phenotypic heterogeneity that can even be found within families.⁴⁸ We hypothesize that the neurodegenerative signature of *C9orf72* at a group level might have resulted from pooling patients with severe but distinct individual degeneration profiles. To investigate this, we analyzed individual neurodegeneration patterns of *C9orf72* mutation carriers from each cluster. Their *Z*-score maps (adjusted for age and sex) reveal heterogeneity within the group of *C9orf72* mutation carriers that is concordant with neurodegeneration patterns of the different clusters (Fig S3). Similarly, despite earlier studies showing *UNC13A* to be related to temporal thinning,⁷ our study did not show a significant association with any of the clusters. Although *UNC13A* and *C9orf72* represent 2 of the most common genetic variants associated with ALS, a more extensive genetic characterization might provide greater insight into the genetic causes of neurodegenerative heterogeneity in our study.

One of the key elements in our findings is that multiple disease aspects corroborate the hypothesis that patients can be categorized into distinct ALS subgroups. The identification of a PM and FT cluster—2 established phenotypes of ALS—supports the validity of the clustering algorithm results. Second, distinct neurodegenerative patterns can be found in the analyses of subcortical structures and cerebellar subfields, even though these imaging parameters were not included in the clustering process. Moreover, the cognitive profiles of the clusters are supportive of the neuroimaging phenotypes, with cognitive impairment predominantly being found in the 2 clusters that show extra-motor neurodegeneration (FT and CPT).

Yet, there are limitations to the study. Due to the nature of the MRI acquisition procedure, we had to exclude patients with severe bulbar or respiratory impairment as these impede lying in a supine position. Still, we aimed to include patients as early as possible (when severe bulbar or respiratory impairment is rare) and managed to include a significant proportion of patients with bulbar onset of symptoms who were still able to participate. The rapidly progressing nature of the disease is a limiting factor in ALS neuroimaging follow-up studies and poses a considerable challenge to creating the large sample size needed to apply machine learning algorithms.⁴⁹ This also, unfortunately, limited the possibility of performing external validation, as our probabilistic clustering method requires large size neuroimaging datasets to produce stable results.

Another limitation is the significant proportion of missing data for cognitive analysis, largely due to the fact that the Dutch version of the ECAS was established in 2015, and detailed cognitive data of patients who participated before 2015 are absent. Although it is possible that the 272 (56%) patients whose ECAS were analyzed could potentially differ from patients included before 2015, we expect this bias to be limited, considering that both the inclusion procedures and MRI scanning protocol remained unchanged over the course of the study. Even though a dataset of this size is probably large enough to have detected clinically significant cognitive changes in the tested domains, no full neuropsychological examination was performed and subtle cognitive changes or cognitive deficits in other domains may have passed undetected.

Due to technical limitations inherent to FACT connectome reconstruction, multiple imputations were needed to equitably perform interpatient comparisons. Because Rubin's rules were used, cross-dataset variance is incorporated in the computation of Pearson's ρ , thus reducing the risk of biased estimates due to imputation. Last, we would highlight that the clustering algorithm is used to identify subtypes of neurodegeneration at a group level and is not designed to accurately classify individual

patients. Subsequent studies may focus on developing tools that could classify individual neurodegeneration subtypes for implementation in clinical practice.

Connectome reconstruction using probabilistic methods may overcome this, but come with other disadvantages (ie, high number of false positives and less accuracy in reconstruction of long-distance connections).

We demonstrate that ALS consists of, at least, 3 distinct subgroups based on patterns of cerebral involvement. These subgroups remain stable during longitudinal assessments and are each associated with distinct clinical characteristics and cognitive profiles. A new neuroimaging phenotype has emerged, besides the pure motor and FTD-like variants, that uniquely exhibits posterior cingulate, parietal, and cerebellar neurodegeneration in addition to motor and temporal involvement. The discovery of this subtype could present a new area of focus for future research and may provide a new approach toward advancing personalized medicine in ALS.

Acknowledgments

The authors would like to thank all participants who volunteered for this study. Furthermore, we would like to thank Simone M.A. Vugts for her efforts in coordinating the study and for her help with data acquisition. This study was funded by the Netherlands ALS Foundation (Stichting ALS Nederland). This project has received funding from the European Research Council (ERC) under the European Union's Horizon 2020 research and innovation program (grant agreement no 772376—EScORIAL).

Author Contributions

All authors contributed to the conception and design of the study. H.H.G.T., H.J.W., A.D.N., K.vV., J.M.M., and H.K.vdB. contributed to the acquisition and analysis of data. H.H.G.T., H.J.W., A.D.N., and L.H.vdB. contributed to drafting the text and preparing the figures.

Potential Conflicts of Interest

The authors report no conflicts of interest.

References

- van Es MA, Hardiman O, Chio A, et al. Amyotrophic lateral sclerosis. *Lancet* 2017;390:2084–2098.
- Westeneng H-J, Debray TPA, Visser AE, et al. Prognosis for patients with amyotrophic lateral sclerosis: development and validation of a personalised prediction model. *Lancet Neurol* 2018;17:423–433.
- Kiernan MC, Vucic S, Talbot K, et al. Improving clinical trial outcomes in amyotrophic lateral sclerosis. *Nat Rev Neurol* 2021;17:1–118.
- Louwerse ES, Visser CE, Bossuyt PMM, Weverling GJ. Amyotrophic lateral sclerosis: mortality risk during the course of the disease and prognostic factors. The Netherlands ALS consortium. *J Neurol Sci* 1997;152:S10–S17.
- Byrne S, Elamin M, Bede P, et al. Cognitive and clinical characteristics of patients with amyotrophic lateral sclerosis carrying a C9orf72 repeat expansion: a population-based cohort study. *Lancet Neurol* 2012;11:232–240.
- van Rheenen W, van Blitterswijk M, Huisman MHB, et al. Hexanucleotide repeat expansions in C9orf72 in the spectrum of motor neuron diseases. *Neurology* 2012;79:878–882.
- Tan HHG, Westeneng H, van der Burgh HK, et al. The distinct traits of the UNC13A polymorphism in amyotrophic lateral sclerosis. *Ann Neurol* 2020;88:796–806.
- van der Burgh HK, Westeneng HJ, Walhout R, et al. Multimodal longitudinal study of structural brain involvement in amyotrophic lateral sclerosis. *Neurology* 2020;94:e2592–e2604.
- Menke RAL, Agosta F, Grosskreutz J, et al. Neuroimaging endpoints in amyotrophic lateral sclerosis. *Neurotherapeutics* 2016;14:1–13.
- Agosta F, Spinelli EG, Filippi M. Neuroimaging in amyotrophic lateral sclerosis: current and emerging uses. *Expert Rev Neurother* 2018;18:395–406.
- Cedarbaum JM, Stambler N, Malta E, et al. The ALSFRS-R: a revised ALS functional rating scale that incorporates assessments of respiratory function. *J Neurol Sci* 1999;169:13–21.
- Abrahams S, Newton J, Niven E, et al. Screening for cognition and behaviour changes in ALS. *Amyotroph Lateral Scler Frontotemporal Degener* 2014;15:9–14.
- Bakker LA, Schröder CD, Spreij LA, et al. Derivation of norms for the Dutch version of the Edinburgh cognitive and behavioral ALS screen. *Amyotroph Lateral Scler Frontotemporal Degener* 2018;20:1–9.
- Balendra R, Jones A, Jivraj N, et al. Estimating clinical stage of amyotrophic lateral sclerosis from the ALS functional rating scale. *Amyotroph Lateral Scler Frontotemporal Degener* 2014;15:279–284.
- Desikan RS, Ségonne F, Fischl B, et al. An automated labeling system for subdividing the human cerebral cortex on MRI scans into gyral based regions of interest. *NeuroImage* 2006;31:968–980.
- Mori S, Crain BJ, Chacko VP, van Zijl PCM. Three-dimensional tracking of axonal projections in the brain by magnetic resonance imaging. *Ann Neurol* 1999;45:265–269.
- Schmidt R, Verstraete E, de Reus MA, et al. Correlation between structural and functional connectivity impairment in amyotrophic lateral sclerosis. *Hum Brain Mapp* 2014;35:4386–4395.
- de Reus MA, van den Heuvel MP. Estimating false positives and negatives in brain networks. *NeuroImage* 2013;70:402–409.
- van Buuren S, Groothuis-Oudshoorn K. mice: Multivariate imputation by chained equations in R. *J Stat Softw* 2011;45:1–67.
- Jeub LGS, Sporns O, Fortunato S. Multiresolution consensus clustering in networks. *Sci Rep* 2018;8:1–16.
- Han S, Carass A, He Y, Prince JL. Automatic cerebellum anatomical parcellation using U-net with locally constrained optimization. *NeuroImage* 2020;218:116819.
- Winkler AM, Ridgway GR, Webster MA, et al. Permutation inference for the general linear model. *NeuroImage* 2014;92:381–397.
- Smith SM, Nichols TE. Threshold-free cluster enhancement: addressing problems of smoothing, threshold dependence and localisation in cluster inference. *NeuroImage* 2009;44:83–98.
- Ravits J, Paul P, Jorg C. Focality of upper and lower motor neuron degeneration at the clinical onset of ALS. *Neurology* 2007;68:1571–1575.
- Devine MS, Kiernan MC, Heggie S, et al. Study of motor asymmetry in ALS indicates an effect of limb dominance on onset and spread of

- weakness, and an important role for upper motor neurons. *Amyotroph Lateral Scler Frontotemporal Degener* 2014;15:481–487.
26. Nitert AD, Tan HH, Walhout R, et al. Sensitivity of brain MRI and neurological examination for detection of upper motor neurone degeneration in amyotrophic lateral sclerosis. *J Neurol Neurosurg Psychiatry* 2022;93:82–92.
 27. Strong MJ, Abrahams S, Goldstein LH, et al. Amyotrophic lateral sclerosis - frontotemporal spectrum disorder (ALS-FTSD): revised diagnostic criteria. *Amyotroph Lateral Scler Frontotemporal Degener* 2017;18:153–174.
 28. Dubois B, Slachevsky A, Litvan I, Pillon B. The FAB: a frontal assessment battery at bedside. *Neurology* 2000;55:1621–1626.
 29. Raaphorst J, Beeldman E, Schmand B, et al. The ALS-FTD-Q: a new screening tool for behavioral disturbances in ALS. *Neurology* 2012;79:1377–1383.
 30. Kasper E, Schuster C, Machts J, et al. Microstructural white matter changes underlying cognitive and behavioural impairment in ALS—an in vivo study using DTI. *PLoS One* 2014;9:e114543.
 31. Chenji S, Ishaque A, Mah D, et al. Neuroanatomical associations of the Edinburgh cognitive and behavioural ALS screen (ECAS). *Brain Imaging Behav* 2021;15:1641–1654.
 32. Agosta F, Ferraro PM, Riva N, et al. Structural brain correlates of cognitive and behavioral impairment in MND. *Hum Brain Mapp* 2016;37:1614–1626.
 33. Christidi F, Karavasilis E, Riederer F, et al. Gray matter and white matter changes in non-demented amyotrophic lateral sclerosis patients with or without cognitive impairment: a combined voxel-based morphometry and tract-based spatial statistics whole-brain analysis. *Brain Imaging Behav* 2018;12:547–563.
 34. Dadar M, Manera AL, Zinman L, et al. Cerebral atrophy in amyotrophic lateral sclerosis parallels the pathological distribution of TDP43. *Brain Commun* 2020;2:fcaa061.
 35. Tan RH, Devenney E, Dobson-Stone C, et al. Cerebellar integrity in the amyotrophic lateral sclerosis-frontotemporal dementia continuum. *PLoS One* 2014;9:e105632.
 36. Bede P, Chipika RH, Christidi F, et al. Genotype-associated cerebellar profiles in ALS: focal cerebellar pathology and cerebro-cerebellar connectivity alterations. *J Neurol Neurosurg Psychiatry* 2021;92:1197–1205.
 37. Tan RH, Kril JJ, McGinley C, et al. Cerebellar neuronal loss in amyotrophic lateral sclerosis cases with ATXN2 intermediate repeat expansions. *Ann Neurol* 2016;79:295–305.
 38. Al-Sarraj S, King A, Troakes C, et al. p62 positive, TDP-43 negative, neuronal cytoplasmic and intranuclear inclusions in the cerebellum and hippocampus define the pathology of C9orf72-linked FTLN and MND/ALS. *Acta Neuropathol* 2011;122:691–702.
 39. Gellersen HM, Guo CC, O'callaghan C, et al. Cerebellar atrophy in neurodegeneration—a meta-analysis. *J Neurol Neurosurg Psychiatry* 2017;88:780–788.
 40. Guell X, Schmahmann J. Cerebellar functional anatomy: a didactic Summary based on human fMRI evidence. *Cerebellum* 2020;19:1–5.
 41. Thomas Yeo BT, Krienen FM, Sepulcre J, et al. The organization of the human cerebral cortex estimated by intrinsic functional connectivity. *J Neurophysiol* 2011;106:1125–1165.
 42. Caga J, Tu S, Dharmadasa T, et al. Apathy is associated with parietal cortical-subcortical dysfunction in ALS. *Cortex* 2021;145:341–349.
 43. Whitwell JL, Przybelski SA, Weigand SD, et al. Distinct anatomical subtypes of the behavioural variant of frontotemporal dementia: a cluster analysis study. *Brain* 2009;132:2932–2946.
 44. Ranasinghe KG, Rankin KP, Pressman PS, et al. Distinct subtypes of behavioral-variant frontotemporal dementia based on patterns of network degeneration. *JAMA Neurol* 2016;73:1078–1088.
 45. O'Connor CM, Landin-Romero R, Clemson L, et al. Behavioral-variant frontotemporal dementia: distinct phenotypes with unique functional profiles. *Neurology* 2017;89:570–577.
 46. Bede P, Bokde ALW, Byrne S, et al. Multiparametric MRI study of ALS stratified for the C9orf72 genotype. *Neurology* 2013;81:361–369.
 47. Westeneng H-J, Walhout R, Straathof M, et al. Widespread structural brain involvement in ALS is not limited to the C9orf72 repeat expansion. *J Neurol Neurosurg Psychiatry* 2016;87:1354–1360.
 48. Floris G, Borghero G, Di Stefano F, et al. Phenotypic variability related to C9orf72 mutation in a large Sardinian kindred. *Amyotroph Lateral Scler Frontotemporal Degener* 2015;17:245–248.
 49. Grollemund V, Pradat PF, Querin G, et al. Machine learning in amyotrophic lateral sclerosis: achievements, pitfalls, and future directions. *Front Neurosci* 2019;13:135.